The Star Formation Newsletter #340 10-18

東大M2 森井嘉穂

10. Clustered star formation towards Berkeley 87 / ON2. I. Multi-wavelength census and the population overlap problem
11. An ALMA Survey of Protoplanetary Disks in Lynds 1641
12. Dispersal timescale of protoplanetary disks in the low-metallicity young cluster Dolidze 25
13. Analysis of physical processes in eruptive YSOs with near infrared spectra and multiwavelength light curves
14. An HST Survey of Protostellar Outflow Cavities: Does Feedback Clear Envelopes?
15. Discovery of an Edge-on Circumstellar Debris Disk Around BD+45598: a Newly Identified Member of the Pictoris Moving Group
16. The Extraordinary Outburst in the Massive Protostellar System NGC6334 I-MM1: Strong Increase in Mid-Infrared Continuum Emission
17. Long-term V (RI)c CCD photometry of pre-main-sequence stars in the association Cepheus OB3
18. MRI-active inner regions of protoplanetary discs. I. A detailed model of disc structure

11. An ALMA Survey of Protoplanetary Disks in Lynds 1641

Sierra L. Grant, Catherine C. Espaillat, John Wendeborn, John J. Tobin, Enrique Macías, Anneliese Rilinger, Álvaro Ribas, S. Thomas Megeath, William J. Fischer, Nuria Calvet, Kyoung Hee Kim ★ We present ALMA observations of 101 protoplanetary disks within the star-forming region Lynds 1641 in the Orion Molecular Cloud A. Our observations include 1.33 mm continuum emission and spectral windows covering the J=2-1 transition of ^{12}CO, ^{13}CO, and C^{18}O. We detect 89 protoplanetary disks in the dust continuum at the 4σ level (~88and 31 in ^{12}CO, 13 in ^{13}CO, and 4 in C^{18}O. Our sample contains 23 transitional disks, 20 of which are detected in the continuum. We target infrared-bright Class II objects, which biases our sample towards massive disks. We determine dust masses or upper limits for all sources in our sample and compare our sample to protostars in this region. We find a decrease in dust mass with evolutionary state. We also compare this sample to other regions surveyed in the (sub-)millimeter and find that Lynds 1641 has a relatively massive dust disk population compared to regions of similar and older ages, with a median dust mass of $11.1^{+32.9}_{-4.6}$ $M_{\oplus}$ and 27masses equal to or greater than the minimum solar nebula dust mass value of ~30 $M_{\oplus}$. We analyze the disk mass-accretion rate relationship in this sample and find that the viscous disk lifetimes are similar to the age of the region, however with a large spread. One object, [MGM2012] 512, shows large-scale (>5000 AU) structure in both the dust continuum and the three gas lines. We discuss potential origins for this emission, including an accretion streamer with large dust grains.

OMC-A Lynds 1641にある101原始惑星系円盤のALMA観測。ダスト連続波で89、^{12}COで31、^{13}COで13、C^{18}Oで4個の円盤を検出。23/101は遷移円盤で20は連続波で受かった。

赤外線で明るい**Class II円盤**に注目。ダスト質量を見積もり、本領域の原始星、他領域と比較した。

→Lynds 1641は比較的大質量なダスト円盤が多い(中央値$11.1^{+32.9}_{-4.6}$ $M_{\oplus}$) 27%はMMSN(~ 30 $M_{\oplus}$)と同等かそれ以上

円盤の質量ー降着率関係を調べ、粘性円盤寿命が領域の年齢と似ていることを明らかにした

[MGM2012]512はダスト連続波でもCO及びその同位体でも>5,000 auの構造が見られ、起源について議論した。大きなダスト粒子の降着流とか

11. An ALMA Survey of Protoplanetary Disks in Lynds 1641

- 惑星を形成するためには円盤は十分な質量もち、物質の散逸前に惑星形成が行われる必要がある(~10 Myr)

- 円盤は小質量星周りでも20%程度
- 原始惑星系円盤のサーベイ観測は様々な領域に対して行われ、
    ✓円盤**質量**が中心星質量や領域の**年齢、進化段階に依存**すること
    ✓星形成環境が円盤進化に影響を与えること
  が明らかになった
- しかし、質量が年齢と単調減少ではないことなどまだ理解は不十分
- 環境と円盤進化において原始惑星系円盤段階の効果を調べるため、様々な進化段階の円盤が多く存在する ひとつの星形成領域を調べる

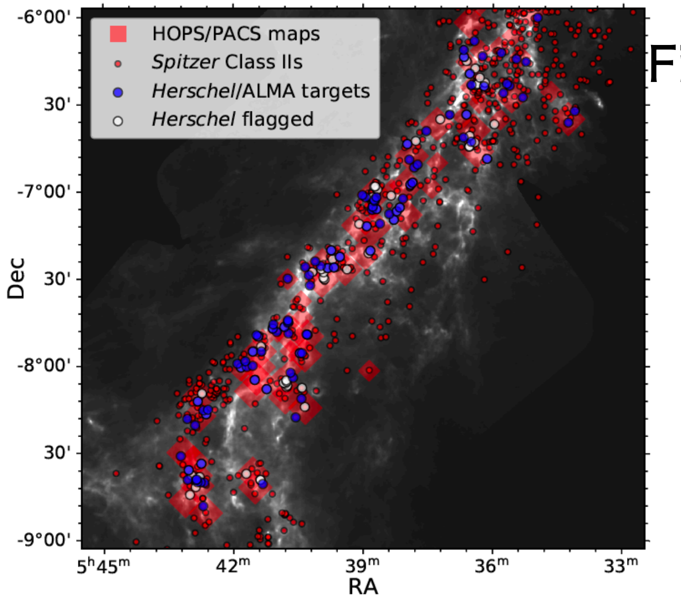

Figure 1

Lynds 1641in Orion A (~1.5 Myr)

Megeath et al. (2012,2016) *Spitzer* survey of Orionで円盤をもつ若い星700天体が同定され、Orion VANDAM survey (Tobin et al. 2020)で新たに165天体も観測された

対象天体 **Class IIの円盤101天体**(Grant et al. (2018)から選抜)、うち23%は遷移円盤

-6°以下のClass II天体(724)のうち、HOPSや70 μmで検出されており、連星間距離が不明or <800 auの連星ではないもの

<注> Herschel では対象領域の全Class II天体を検出していない(本研究に入っていない) & HOPSで観測されているのはクラスター/フィラメント領域で、散らばって分布するClass II天体は含まれていない

→本研究の対象天体は若く、赤外で明るく、おそらく大質量をもつ、Class IIの中でも初期の円盤

観測 ALMA Cycle 7, Band 6 (CO, ^{13}CO, C^{18}O (J=2-1)), ~1.3″×1.0″

11. An ALMA Survey of Protoplanetary Disks in Lynds 1641

結果1. 連続波

- イメージベースでGaussian fitしmaximum flux > 4 rms →**検出**(89/101)
- Gaussian天体を仮定した‘uvmodelfit’を行い、長軸FWHM、長短軸比、position angle、fluxを測定
- S/N > 30 かつGaussian天体を仮定した場合のフラックス密度 > (点源を仮定した場合のフラックス密度+3 sigma)→**分解** (13/89)

質量 $M_{\rm dust} = \dfrac{d^2 F_\nu}{\kappa_\nu B_\nu(T_{\rm dust})}$ $(\kappa_\nu = (\nu/100\ {\rm GHz}) = 2.254\ {\rm cm^2 g^{-1}}, {\rm T} = 20\ {\rm K})$

中央値は$\mathbf{11.1^{+32.9}_{-4.6}}$ $\boldsymbol{M_\oplus}$、transition disk(20/23)は16.1 $M_\oplus$

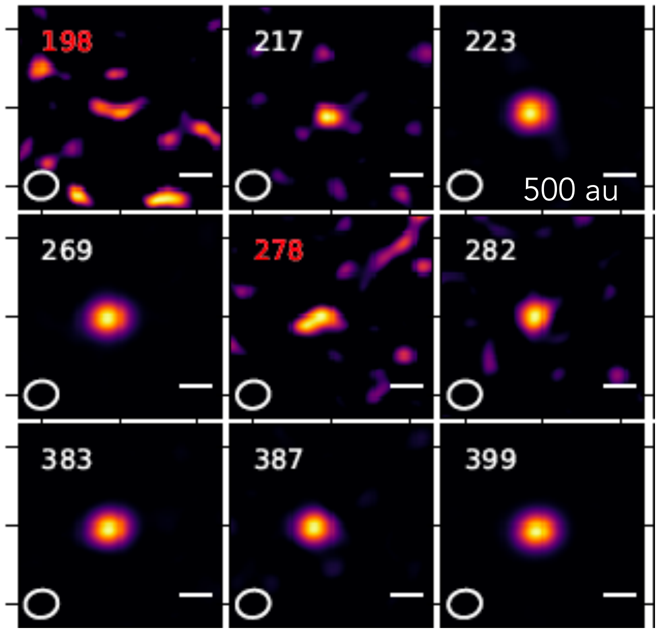

Figure 2

赤字はnon-detectionを意味

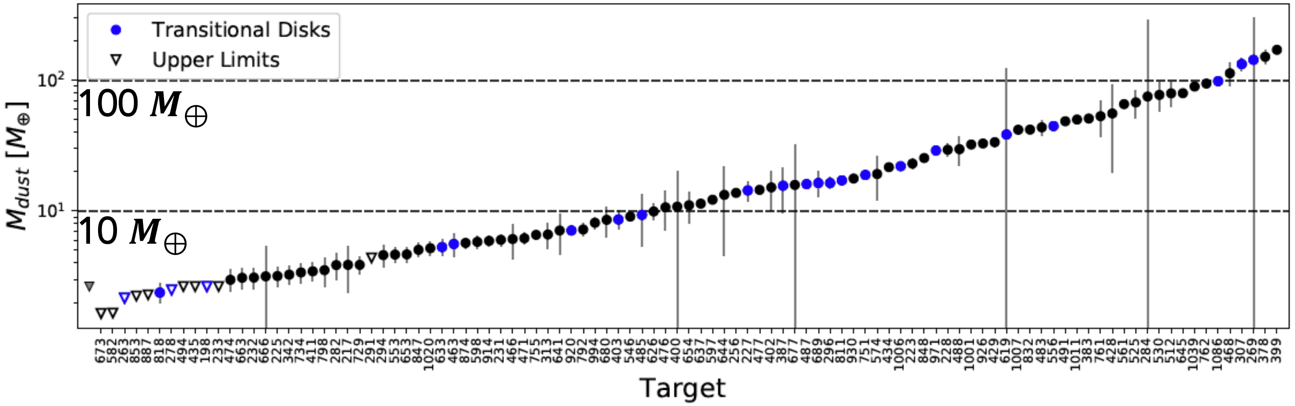

Figure 5 Blues: transition disks

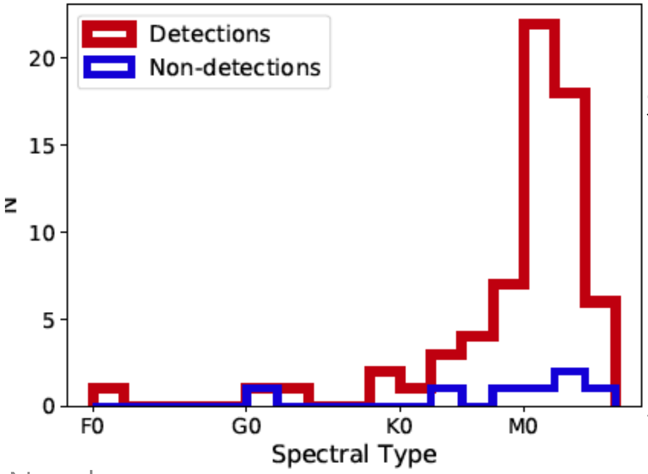

Figure 4

本観測で最も多いのはM1 (Teff=3680, ~0.4-0.5 $M_\odot$, 1Myrの前主系列星)

L1641内で最も多いのはより後期段階のM4 (Hsu et al. 2012, Fang et al. 2013) →サンプルバイアス

11. An ALMA Survey of Protoplanetary Disks in Lynds 1641

他の進化段階にある領域とL1641の結果を比較 (本解析で用いた温度とκで質量を再計算)

VANDAM survey (同じ領域, ~1.5 Myr), ONC, OMC1, 2, Ophiuchus (1 Myr), Lupus, Corona Australis (1-3 Myr), Chamaeleon I, Taurus (2 Myr), IC 348 (2-3 Myr), **σ** Ori (3-5 Myr), and Upper Scorpius (5-11 Myr)

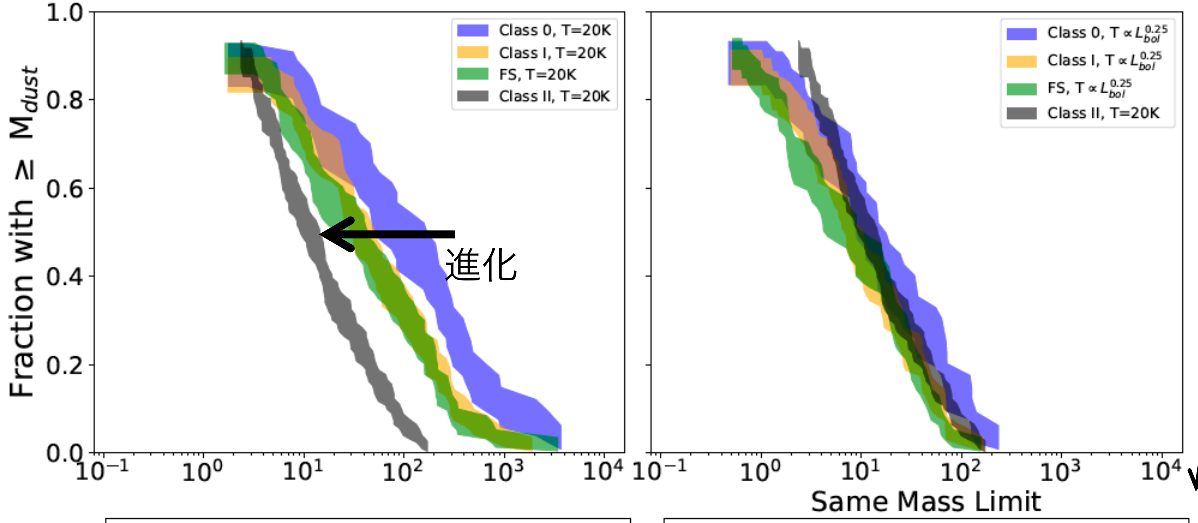

Figure 6

本観測とVANDAM surveyの比較

(左)温度とκを統一

(右)温度はL_{bol}に基づいたもの(Tobin et al. 2020)

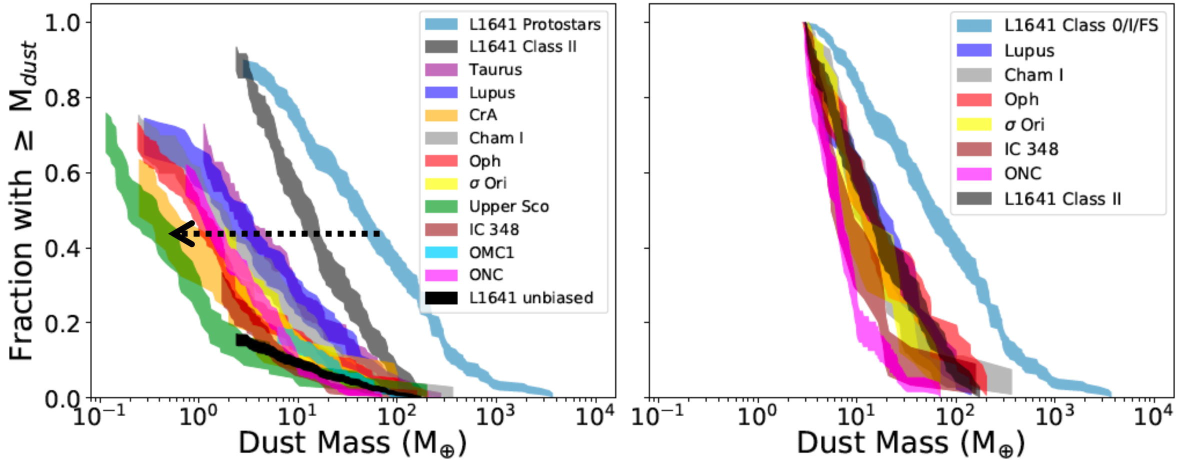

Figure 7

本観測と様々なsurveyの比較

(左)

- 最も老いた領域(Upper Scorpius)が小質量側、若いVANDAM原始星円盤が大質量側に位置
- 本観測(L1641 Class II)は検出率の高さと比較的大質量な円盤を検出したことが分布の原因
- L1641 unbiasedは70 μmの観測がされていない(本観測に入っていない)天体を考慮した場合(質量は上限値)→unbiased surveyの必要性

(右) 感度による違いをなくすため、2.8 $M_\oplus$を下限とした場合

- L1641Class IIは他と大きく違わない

11. An ALMA Survey of Protoplanetary Disks in Lynds 1641

Figure 8　本観測と様々なsurveyの質量分布の比較

- 年齢が増えるほど質量は低い方にシフト
- L1641のサンプルバイアスを考慮するとより低質量側にシフトする
- L1641 Class IIの分布はOMC1,2, Taurusと似ている
- ピークはUpper ScorpiusとCorona Australisが数桁大質量側にシフトしている

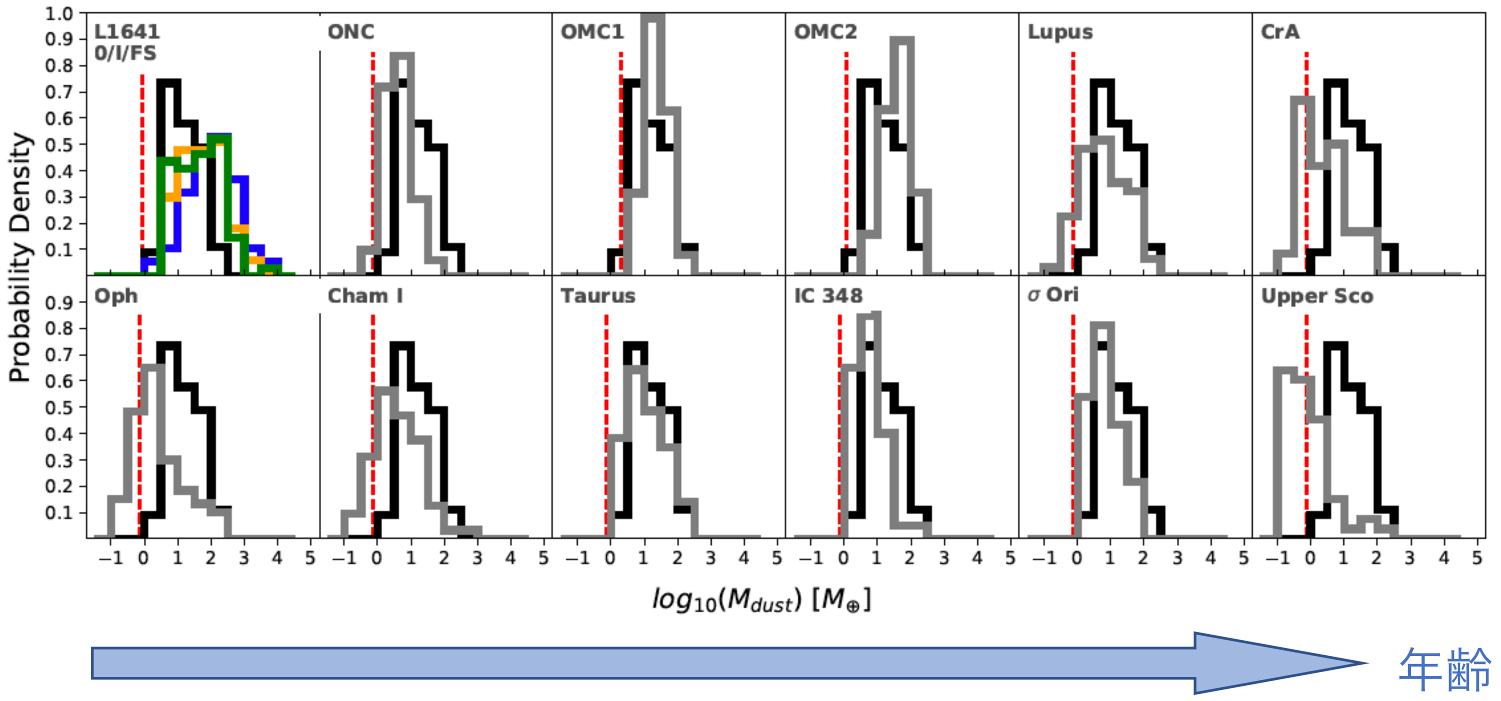

黒 L1641 Class II
灰 ALMA survey
青 Class 0
橙 Class I
緑 Flat

赤線　検出された中で最も
低質量なダスト円盤質量

11. An ALMA Survey of Protoplanetary Disks in Lynds 1641

<u>結果2. CO</u> イメージベースでGaussian fit+目視で検出を判断 → ^{12}COで31、^{13}COで13、C^{18}Oで4つの円盤を検出

ガス質量を求めるには^{13}COとC^{18}Oが必要だが、3天体しかないので断念

Figure 9

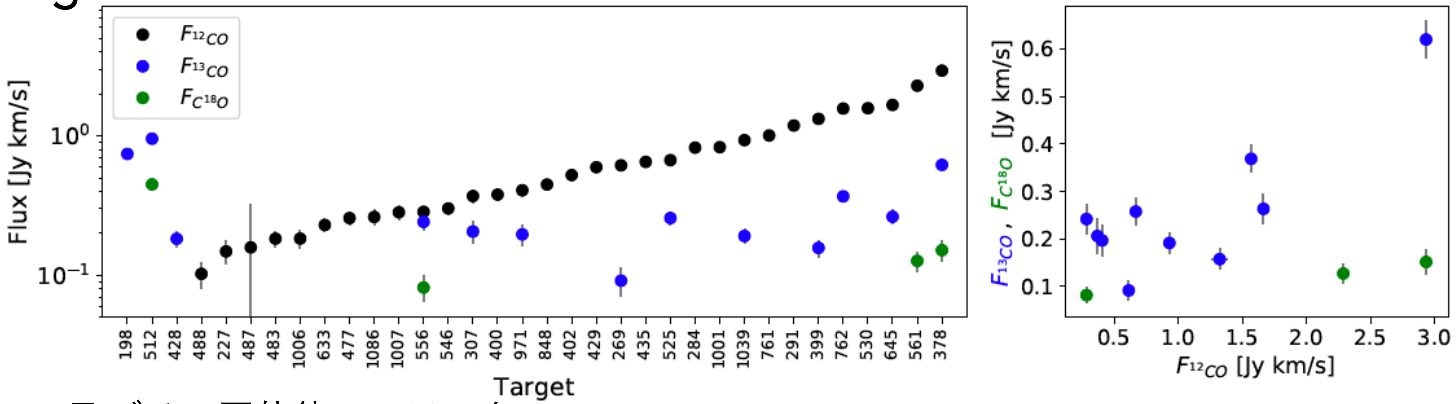

CO及びその同位体のフラックス

^{12}COと^{13}COの間はPearsonの相関係数は0.82、**C^{18}O**とは0.99の強い相関が見られた

連続波と^{12}COの間の相関係数は0.56で、連続波とC^{18}O, ^{13}COの間には相関なし

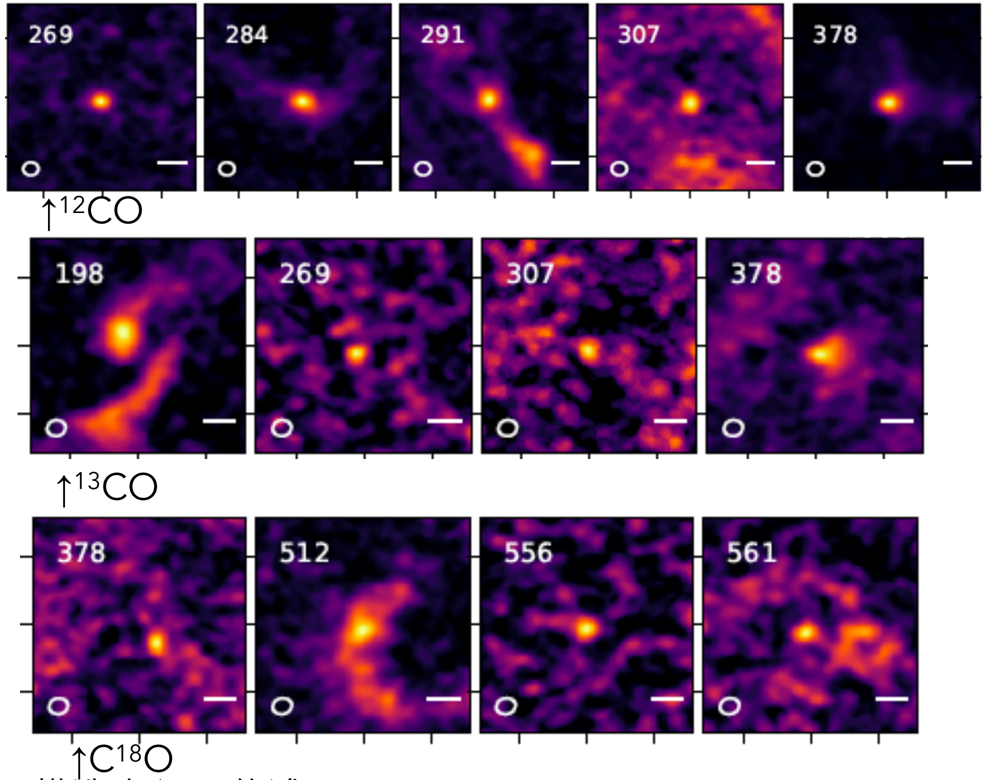

Figure 13 [MGM2012] 512 (M5.5 ± 0.9)

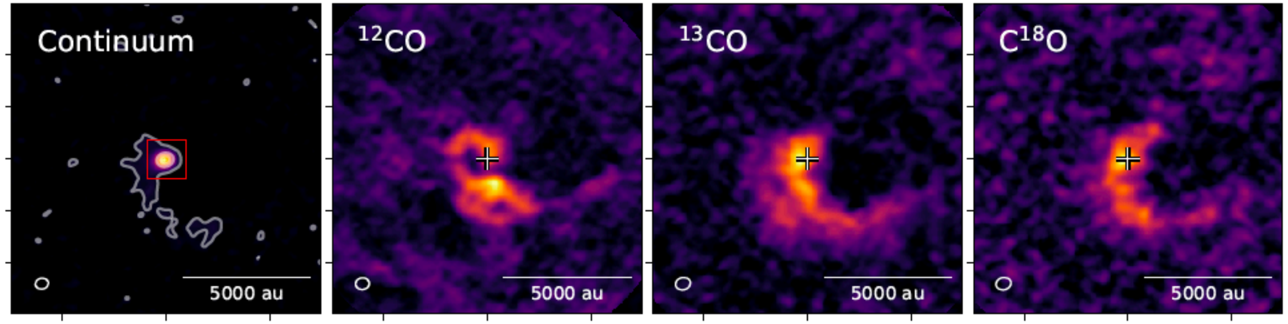

✓ 南側にarc構造(起源は後述)

✓ ^{12}COではおそらく自己吸収による穴がみられる

✓ 広がった成分のダスト質量は円盤質量の約50%($65 \pm 32\ M_{\oplus}$)

✓ エンベロープ成分だとすると、envelope/disk 比からJørgensen et al. (2009)の分類ではClass Iに分類される

<注意>式１がarcの質量の見積もりに適しているか不明。円盤質量は光学的に厚い場合低く見積もっている可能性あり。

11. An ALMA Survey of Protoplanetary Disks in Lynds 1641

議論1. L1641とオリオン内の他の領域

ONC 低質量な円盤(Eisner et al. 2018)

OMC2(ONCの北部、より低い星密度) 小質量星形成領域と同様の円盤populations (Terwisga et al. 2019)

L1641(ONCより低密度、低い背景放射) 1600以上のClass II, III天体(ONCと同程度)

✓ L1641は若いONC領域、より老いたσ Oriよりも**大質量なダスト質量分布**(OMC1に類似、OMC2よりわずかに低質量)

→ダスト質量分布は、領域の年齢、進化段階、外からの光蒸発などに依存

惑星形成のタイミング

若い系のALMA観測から、Class IIに進化するまでにダスト質量は急減すると提案されている。

PerseusのClass 0, I円盤のサーベイからは、Class 0段階に惑星形成が始まるなら必要な惑星形成効率は15%、Class I段階からの場合30%と示唆(Tychoniec et al. 2020)→Class II段階からの場合より厳しい

Grant et al. (2018)はHerschelの観測からL1641でダストが育っていることを発見

✓ しかし、本観測で検出した円盤のうち27%が30 $M_{\oplus}$より大質量(中央値11.1 $M_{\oplus}$はPerseusのClass 0, I円盤質量くらい)

→ L1641の大質量円盤は、たとえ低い効率でも、巨大惑星を形成できるかもしれない

11. An ALMA Survey of Protoplanetary Disks in Lynds 1641

議論2. 遷移円盤

古典的にはClass II円盤とClass II円盤の間に位置する段階の円盤と考えられていた

が、Ansdell et al. (2016)やvan der Marel et al. (2018)はtransition diskがミリ波で明るいことを発見(大質量円盤を示唆)

→異なる進化パスをもつ天体？(惑星の形成やcondensation frontによるリング形成→large cavityの生成)

✓ 本研究で見積もったtransition diskの質量は全体平均よりわずかに大きいが、統計的には似ていた

<注意> cavityの成分により過大評価している可能性あり

✓ SEDにより判断した以外にもサンプルはあるかもしれない

✓ 高解像度観測により、gapが検出できるかもしれない(SEDではdipが見えている)

Figure 14

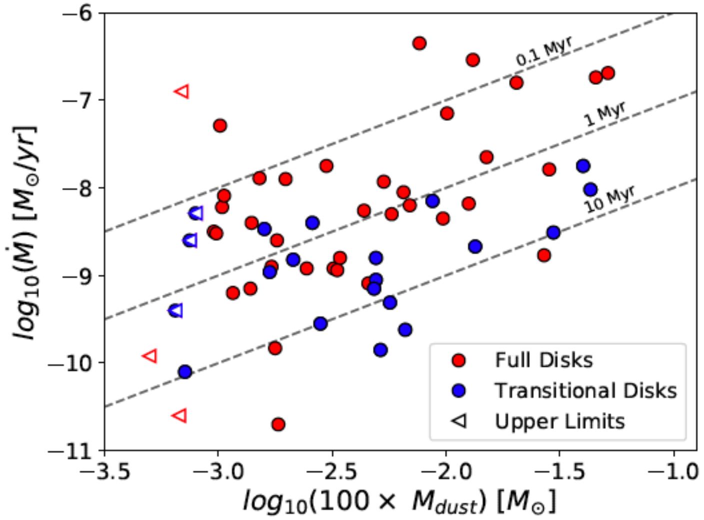

議論3. 質量ー質量降着率

質量降着率はFang et al. (2009, 2013) and Kim et al. (2016)から引用

log-log space で相関係数は0.44 (transition diskは0.42)

点線はviscous lifetime $t_{disk} = M_{disk} / \dot{M}$ 散らばりはあるが、概ね~1.5 Myr

散らばりの原因：降着率の変動性、距離の不定性、光蒸発や惑星形成がもたらす降着率への影響、envelopeからのinfallなど

11. An ALMA Survey of Protoplanetary Disks in Lynds 1641

議論4. [MGM2012] 512のarc構造

エンベロープ/降着 streamerやoutflow cavity、見えていない摂動などが起源？

ローカル環境からの質量獲得による構造は他の天体で見られている(Per-emb-2, [BHB2007]1, SU Aur, HL Tau)

この天体が特殊なのは、連続波でも検出されていること(→ダストサイズは100 μm以上を示唆)

もし、この放射がaccretion streamerなら、ダスト粒子は物質がエンベロープや円盤に落ち込む時に成長できることを意味

定量的には小質量雲の分裂片がYSOと相互作用する流体力学モデル(→accretion burstの可能性を示唆)や非理想MHDモデル (Lebreuilly et al. 2020) (←ダストが成長している観測事実と一致)と似ている。

Figure 15

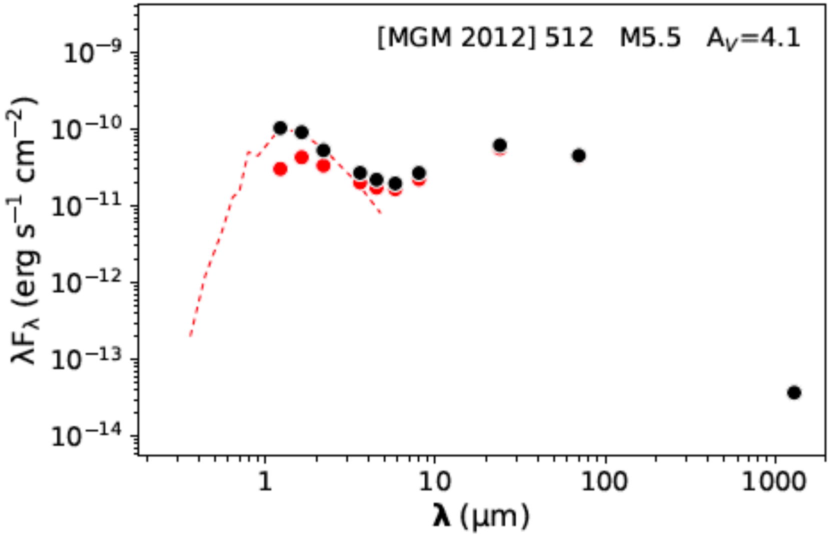

原始星なのか前主系列星なのか

- SEDはenvelopeの存在を示唆
- Whitney et al. (2003)ではClass I 後期に対応→pole-onでみた原始星? 光球+disk/envelope
- 2.2-24 μmのspectral indexを用いた分類ではClass I (Caratti o Garatti et al. 2012) ↑前景放射に敏感
- Megeath et al. (2012)は3.6-4.5 μmのspectral indexから円盤を伴う前主系列星と分類

どちらにせよ境界に近いだろう

Figure 15. The spectral energy distribution of [MGM2012] 512. The red points are the observed photometry and the black points are the dereddened data given a visual extinction of 4.1 mag. The red-dashed line is the photosphere for an M5.5 star from Kenyon & Hartmann (1995), scaled to the J-band. There is a large excess at mid- and far-infrared wavelengths, potentially due to envelope emission.

14. **An HST Survey of Protostellar Outflow Cavities: Does Feedback Clear Envelopes?**

Nolan M. Habel, S. Thomas Megeath, Joseph Jon Booker, William J. Fischer, Marina Kounkel, Charles Poteet, Elise Furlan, Amelia Stutz, P. Manoj, John J. Tobin, Zsofia Nagy, Riwaj Pokhrel, Dan Watson ★ We study protostellar envelope and outflow evolution using Hubble Space Telescope NICMOS or WFC3 images of 304 protostars in the Orion Molecular clouds. These near-IR images resolve structures in the envelopes delineated by the scattered light of the central protostars with 80 AU resolution and they complement the 1.2-870 micron spectral energy distributions obtained with the Herschel Orion Protostar Survey program (HOPS). Based on their 1.60 micron morphologies, we classify the protostars into five categories: non-detections, point sources without nebulosity, bipolar cavity sources, unipolar cavity sources, and irregulars. We find point sources without associated nebulosity are the most numerous, and show through monochromatic Monte Carlo radiative transfer modeling that this morphology occurs when protostars are observed at low inclinations or have low envelope densities. We also find that the morphology is correlated with the SED-determined evolutionary class with Class 0 protostars more likely to be non-detections, Class I protostars to show cavities and flat-spectrum protostars to be point sources. Using an edge detection algorithm to trace the projected edges of the cavities, we fit power-laws to the resulting cavity shapes, thereby measuring the cavity half-opening angles and power-law exponents. We find no evidence for the growth of outflow cavities as protostars evolve through the Class I protostar phase, in contradiction with previous studies of smaller samples. We conclude that the decline of mass infall with time cannot be explained by the progressive clearing of envelopes by growing outflow cavities. Furthermore, the low star formation efficiency inferred for molecular cores cannot be explained by envelope clearing alone.

OMCの原始星304天体のエンベロープとアウトフローをHubble Space Telescope 画像を用いて調べた。近赤外線画像は中心星の散乱光からエンベロープ内の構造を80 auの分解能で分解。1.60 μmの形態に基づき、(1)未検出(2)点源(3)双極キャビティ(4)単極キャビティ(5)不規則に分類。(2)が最も多かった

SEDから決めた進化段階と分類に相関があり、Classs 0原始星はほとんんど(1)で、Class Iは(3)や(4)、flatは(2)

キャビティの形状をフィットしたが、原始星の進化に伴うキャビティの成長は見られなかった→進化とともに質量流入が低下することや、低い星形成効率はアウトフローキャビティの成長によるエンベロープの除去(だけ)では説明できなさそう。

Q エンベロープ密度がClass 0段階からflat-spectrum段階の間に1/50倍になる(Furlan et al. 2016)→Class Iで急減?

Q アウトフローのフィードバックでエンベロープは取り除かれ、infallは止まるのか

Q アウトフローキャビティと進化段階の関係は？

HOPS天体のHSTでの観測(80 au)からキャビティを空間分解し、進化段階との関係を調べた

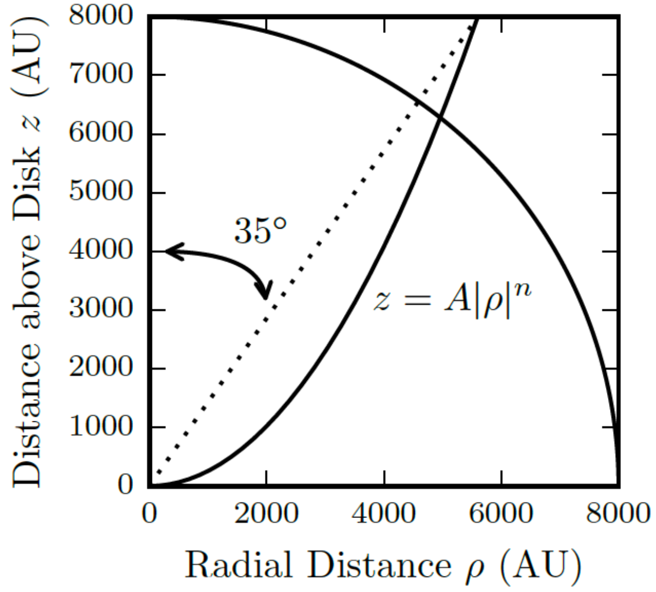

Figure 1. The definition of the cavity half-opening angle used in this paper and in the HO-CHUNK code. The circular region is the outer radius of the envelope of the protostar in these models, set to 8000 AU; the parabolic ($n = 2$) black line is the adopted boundary of the evacuated outflow cavity. The central protostar is located at the origin. The cavity half-opening angle is defined by the angle between the dotted line intersecting the cavity at 8000 AU above the normal to the disk and the polar axis.

Table 1. Parameters used in the model grid described in Section 3.

Parameter	Value(s)
R_{star}: Radius of star	$2.09\,R_\odot$
Temperature of central star	4.0×10^3 K
Mass of central star	$0.5\,M_\odot$
Minimum disk radius	$7.00\,R_{star}$
Disk Scale height at R_{star} [a]	0.018 AU
Maximum envelope radius	8000 AU
Minimum envelope radius	$6.85\,R_{star}$
Degree of polynomial shape of cavities	2.0
Height of cavity wall at $\rho = 0$	$0\,R_{star}$
Density of the cavity	$0\,g\,cm^{-3}$
Ambient cloud density	$0\,g\,cm^{-3}$
Minimum radius of outflow	0.1 AU
Maximum disk radius	5, 50, 100, 200 and 300 AU
Centrifugal radius	Always equal to maximum disk radius
Mass of disk	0.001, 0.005, 0.01 and 0.05 $M_\odot$
α_{disk}: Radial exponent in disk density law	2.125 and 2.25
β_{disk}: Vertical exponent in disk density law	$\alpha_{disk} - 1$
Mass infall rate [b]	1×10^{-7}, 5×10^{-7}, 1×10^{-6}, 5×10^{-6}, 1×10^{-5} and $5 \times 10^{-5}\,M_\odot\,yr^{-1}$
Half-opening angle of inner cavity wall	5°, 15°, 25°, 35° and 45°
Angle of inclination measured from polar axis	1°, 10°, 20°, 30°, 40°, 50°, 60°, 70°, 80° and 90°

$\dot{M}$(envelope density)
opening angle
inclination angle

model

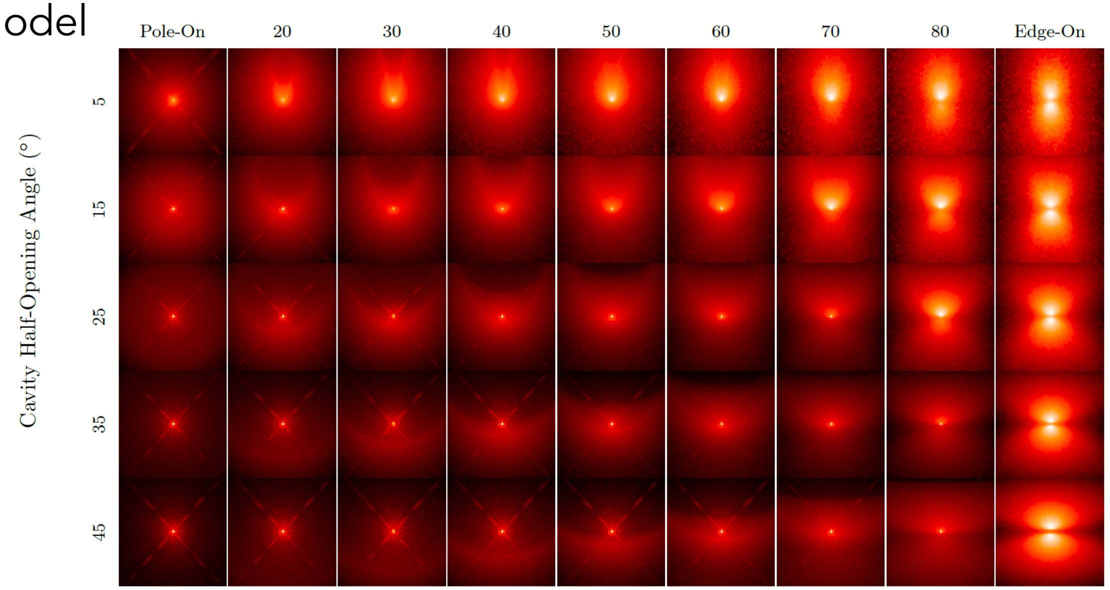

Figure 2. A selection of models from the grid used in this work, showing variations in the observed scattered-light morphologies from models with a mass infall rate of 5×10^{-6} $M_\odot$ yr^{-1}. Note that the contrast between the cavity and the central point source is highest when observed at an inclination greater than the half-opening angle. Each model is shown with an approximately 8000 by 8000 AU field of view.

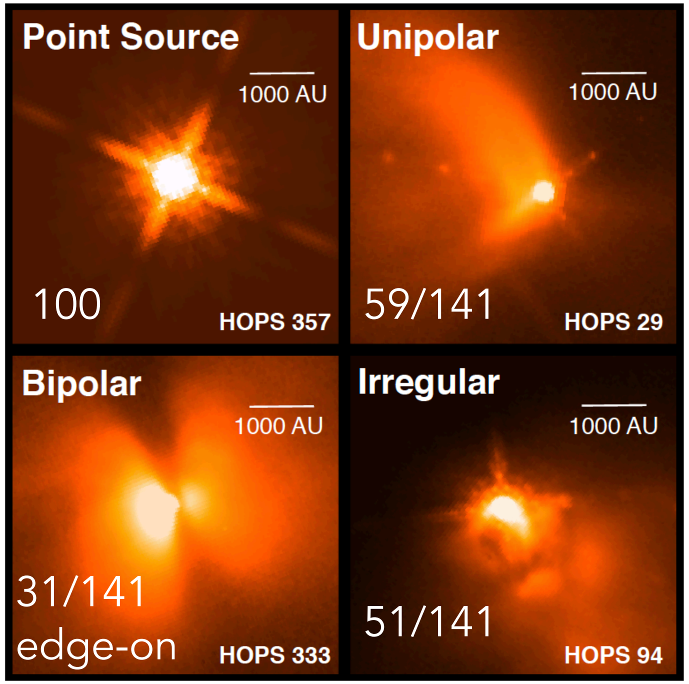

Table 2. Breakdown of F160W morphologies

	Point Source	No Point Source	Total
Non-detections	-	60+3	60+3[a]
Point Source[b]	93+7	-	93+7[c]
Irregular	39	12	51
Unipolar	36	23	59
Bipolar	16	15	31
Total	184+7	110+3	294+10[d]

←観測-分類 全304天体

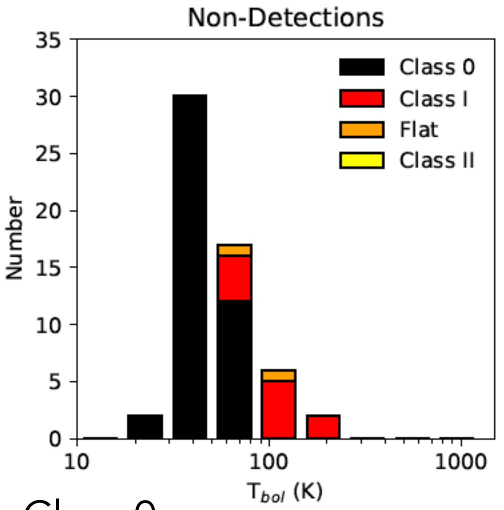

Class 0
optical depthの影響

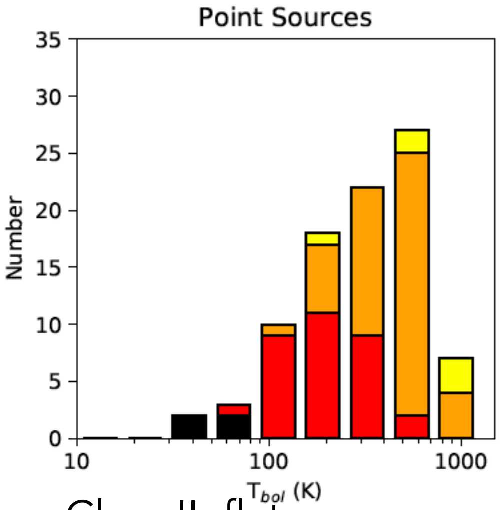

Class II, flat
ダスト密度の低さ

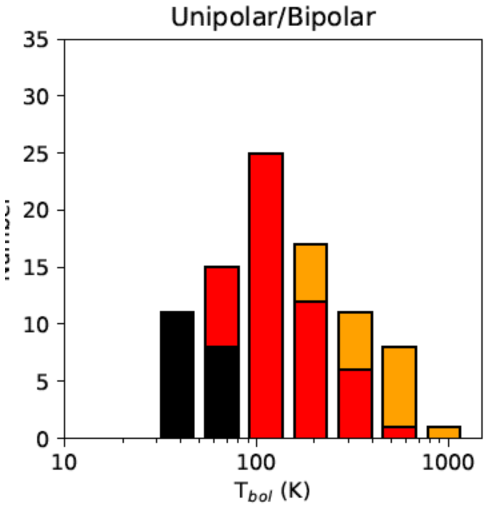

Class 0, Iが多い

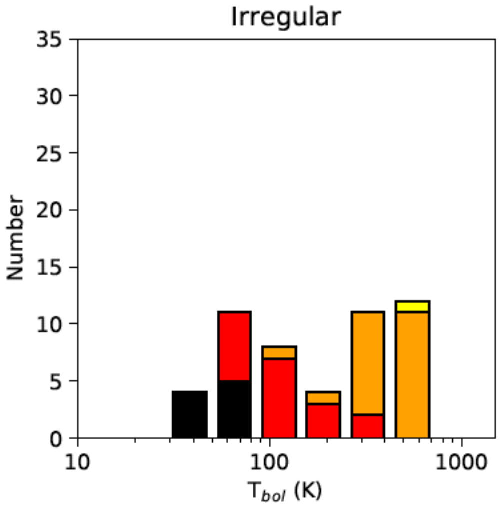

Class II, flat多め

観測から得たedge
モデルのcavity wall

I(x+2)-2I(x+1)+I(x)=0

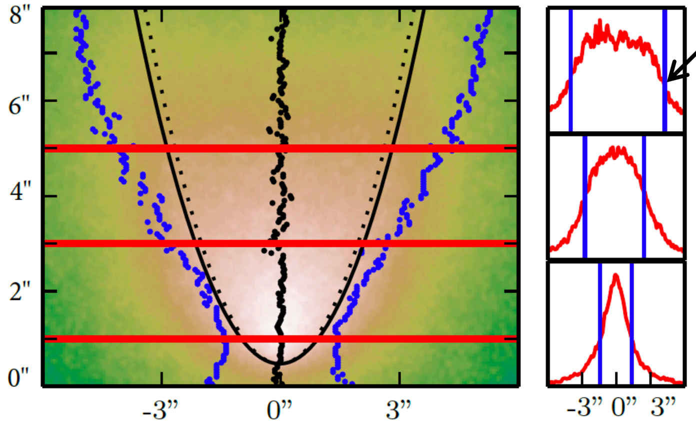

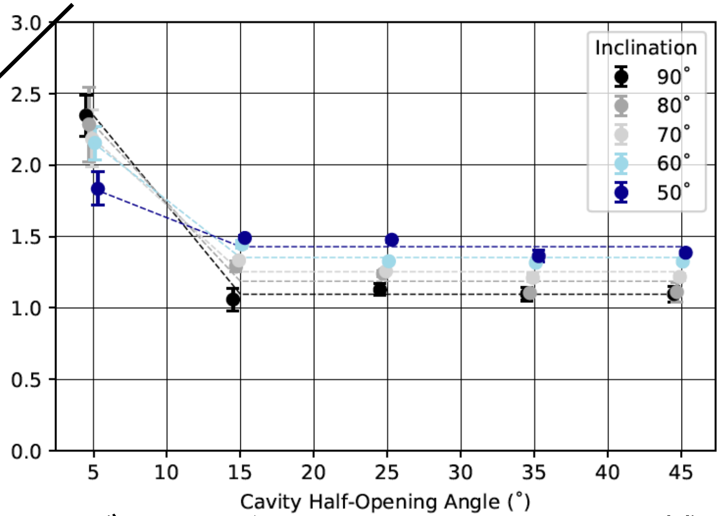

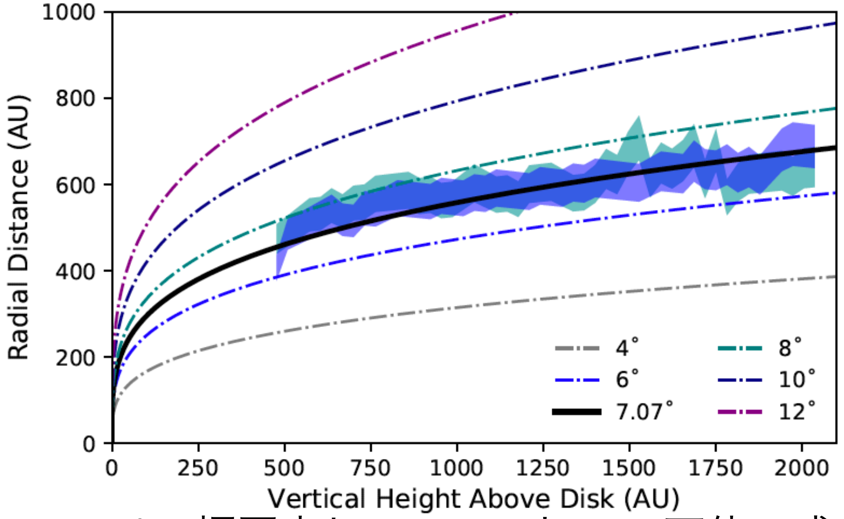

1. スライスしてedgeを探す

2. モデルから得たcorrection ratioで補正

3. edge幅固定してフィット→30天体で成功

$$y = A|x - x_0|^n + y_0$$

振幅Aとcavity half-opening angle θから
エンベロープ半径Rが決まる

$$A = R_{\max}^{1-n} \cot^n \theta$$

Cavity Half-Opening Angle (°)

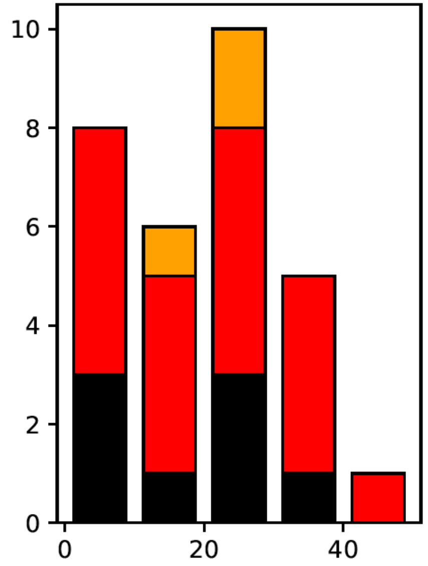

Volume Fraction Cleared

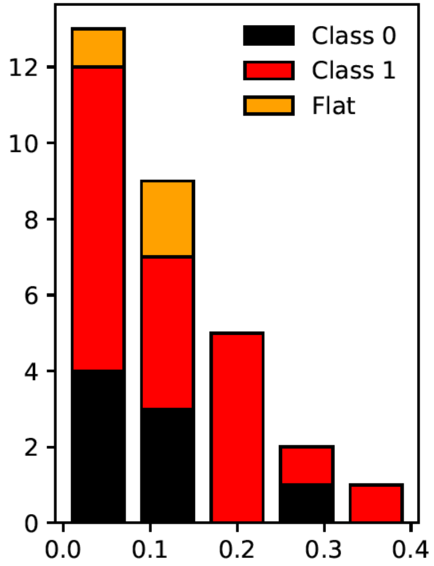

Table 3. Spearman Coefficients and p-values.

Evolutionary Diagnostic	vs Half-Opening Angle r	vs Half-Opening Angle p-value	vs Volume Fraction r	vs Volume Fraction p-value
$T_{\rm bol}$	0.24	0.20	0.23	0.21
$\dot{M}_{\rm infall}$	0.16	0.41	0.12	0.52
$L_{\rm bol}$	0.26	0.16	0.29	0.12

L_{bol}とキャビティの大きさに相関あり？
ほぼClass I天体という影響大

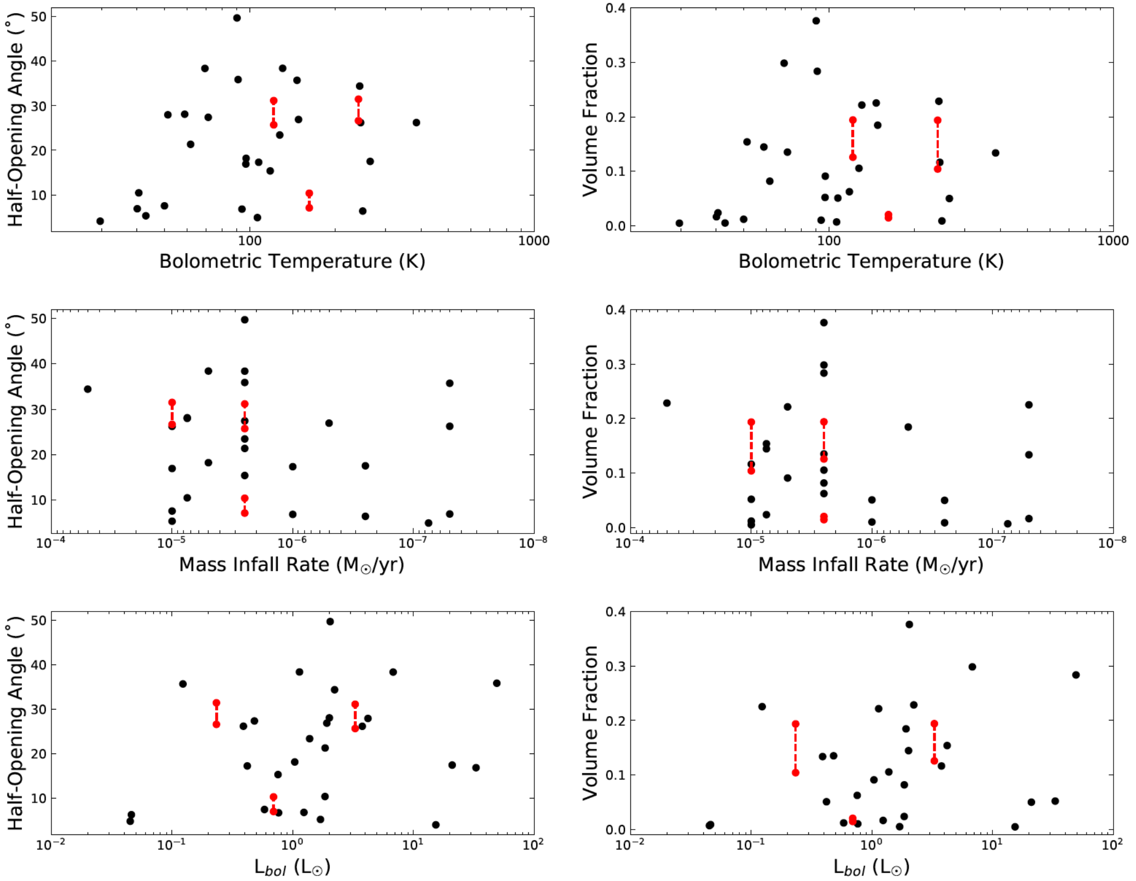

5-50°のopening angleがT_{bol}や降着率に依らず検出
→エンベロープ進化はアウトフローキャビティーの
成長に駆動されていない

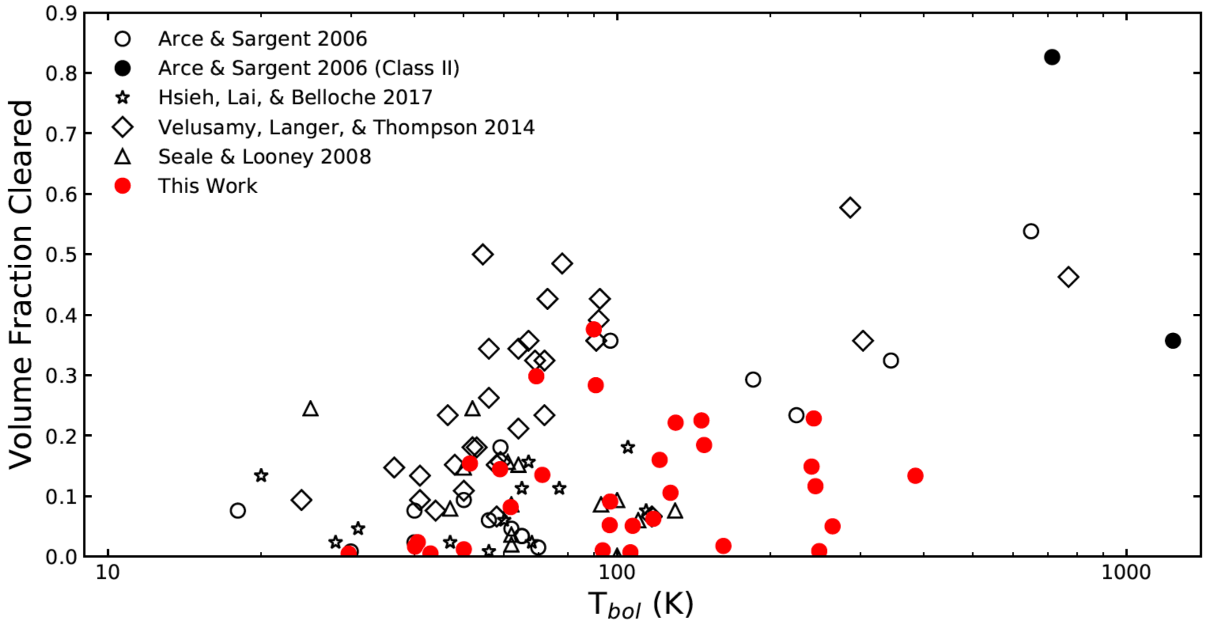

Arce & Sargent (2006) 相関あり(Class IIを考慮した場合)
Velusamy et al. (2014) T_{bol}<100 Kでクリアな増加
Seale & Looney (2008) 相関なし
Heish et al. (2017) Class 0でトレンドあり
本研究ではClass 0が少なかったこともあり相関なし

最大でもClass I後期段階でアウトフローで取り除かれる体積は40%
→エンベロープ密度の急減はアウトフローのフィードバックのみで　説明するのは難しい
低い星形成効率(30-40%)を説明するにも不十分

<注>巻き上げられたガス全てを散乱光で測定できているとは限らない

16. **The Extraordinary Outburst in the Massive Protostellar System NGC6334I-MM1: Strong Increase in Mid-Infrared Continuum Emission**

T. R. Hunter, C. L. Brogan, J. M. De Buizer, A. P. M. Towner, C. D. Dowell, G. C. MacLeod, B. Stecklum, C. J. Cyganowski, S. J. El-Abd, B. A. McGuire ★ In recent years, dramatic outbursts have been identified toward massive protostars via infrared and millimeter dust continuum and molecular maser emission. The longest lived outburst (> 6 yr) persists in NGC6334I-MM1, a deeply-embedded object with no near-IR counterpart. Using FORCAST and HAWC+ on SOFIA, we have obtained the first mid-infrared images of this field since the outburst began. Despite being undetected in pre-outburst ground-based 18 μm images, MM1 is now the brightest region at all three wavelengths (25, 37, and 53 μm), exceeding the ultra-compact HII region MM3 (NGC6334F). Combining the SOFIA data with ALMA imaging at four wavelengths, we construct a spectral energy distribution of the combination of MM1 and the nearby hot core MM2. The best-fit Robitaille radiative transfer model yields a luminosity of $(4.9 \pm 0.8) \times 10^4 L_\odot$. Accounting for an estimated pre-outburst luminosity ratio MM1:MM2 = 2.1 ± 0.4, the luminosity of MM1 has increased by a factor of 16.3 ± 4.4. The pre-outburst luminosity implies a protostar of mass 6.7 $M_\odot$, which can produce the ionizing photon rate required to power the pre-outburst hypercompact HII region surrounding the likely outbursting protostar MM1B. The total energy and duration of the outburst exceed the S255IR-NIRS3 outburst by a factor of $\gtrsim 3$, suggesting a different scale of event involving expansion of the protostellar photosphere (to $\gtrsim 20$ $R_\odot$), thereby supporting a higher accretion rate ($\gtrsim$0.0023 $M_\odot$ yr^{-1}) and reducing the ionizing photon rate. In the grid of hydrodynamic models of Meyer et al. 2021, the combination of outburst luminosity and magnitude (3) places the NGC6334I-MM1 event in the region of moderate total accretion ($\sim$0.1-0.3 $M_\odot$) and hence long duration ($\sim$40-130 yr).

NGC6334I-MM1におけるアウトバースト。UC HII regionのMM3よりも明るい(25, 37, 53 μm)

アウトバースト前後でluminosityは16倍に。アウトバースト前の明るさは、HC HII regionを駆動するのに必要な電離光子率を生み出せる6.7 $M_\odot$の原始星を示唆

流体モデルによると、MM1のイベントは長い継続時間(~40-130年)をもつ

- FU Ori (Class 0)に始まり、20個をこえるClass I, II の小質量原始星でアウトバーストが確認されている

→星がゆっくりと連続した降着と急速で間欠的な降着で形成されていることを示唆

- アウトバーストの間隔は数ヶ月から数百年まで様々
- 大質量YSO(S255IR-NIRS3)でも2年ほど続くアウトバーストが確認された(Caratti o Garatti et al. 2017; Liu et al. 2018)
- 大質量原始クラスター**NGC 6334 I** (d~1.3 kpc)でもALMAを用いて2015年にアウトバーストが発見された

- **MM1, MM2** extremely line-rich hot molecular cores, (HC)HII region (→MM1B, MM2B), bipolar outflows
- **MM3** (UC)HII region NGC6334F
- MM1B を中心としたミリ波アウトバースト
- HartRAO 26m telescopeで2015年1月から複数のメーザーでフレアが観測された→降着イベントを示唆
- ALMAとHartRAOによる継続的な観測では、強まった連続波とメーザー放射が継続
- MM1周囲でのアウトバーストの結果、VLAで強い6.7 GHzメタノールメーザーが検出された
- この論文ではアウトバーストが始まって初の中間赤外線イメージをALMAの結果とともに紹介する

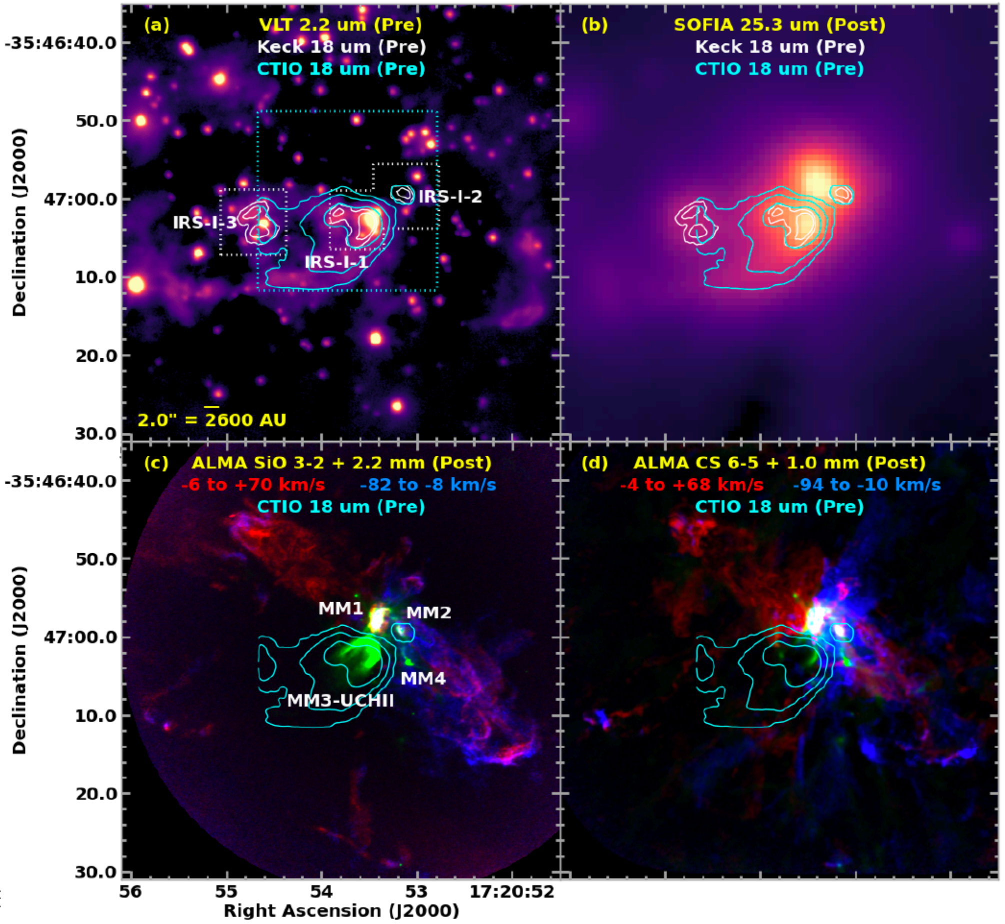

観測データ

1. SOFIA 近赤外 Level 4 (FORCAST 25 and 37 μm) and Level 3 (HAWC+ 53 μm)
2. ALMA Band 4, 7, 8, and 9 (2.2, 1.0, 0.76, and 0.43 mm) within 8 months
3. HartRAO メーザー放射
4. アーカイブデータ

Table 2. Multi-wavelength astrometry and photometry

Observatory	Mean wavelength (μm)	Resolution ($''$)	Shift applied ΔRA($''$), ΔDec($''$)	Flux density[a] (Jy)	Mean epoch
Data taken prior to the outburst					
VLT	2.15	0.6	0.0, 0.0[b]	$< 5.3 \times 10^{-6}$	2012.44
Keck	10	0.33	+1.08, −1.59	0.13±0.01	1999.32
CTIO	18	1.0	+1.65, +0.14	3.49±0.57	1998.50
Keck	18	0.41	+1.08, −1.59	3.43±0.35	1999.32
Herschel PACS (HOBYS)	70	5.9	+0.0, −2.0	2260±452	2010.92
SMA[c,d] (VEX + EXT)	878	0.54×0.28, +9°	+0.12, +0.12	14.6±1.6	2008.12
SMA[c] (VEX)	1326	0.80×0.34, +18°	+0.06, +0.4	4.0±0.41	2008.63
Data taken since the outburst began in 2015					
VVV/VVVX	2.15	0.7 – 1.0	0.0, 0.0	$< 4.2 \times 10^{-6}$	2017.15
SOFIA FORCAST	25.3	3.2	+0.5, +0.5	1014±129	2019.52
SOFIA FORCAST	37.1	3.5	+0.25, +0.25	3604±447	2019.52
SOFIA HAWC+	53	5.6	+0.5, +0.5	7661±1246	2018.53
ALMA	432	0.31×0.17, −76°	0.0, 0.0	346±51	2018.65
ALMA	758	0.31×0.19, +89°	0.0, 0.0	65.5±9.7	2018.70
ALMA	1005	0.33×0.28, +61°	0.0, 0.0[e]	31.7±3.2	2018.38
ALMA	2173	0.32×0.24, −81°	0.0, 0.0	2.90±0.29	2018.08

[a] Value from the apertures shown in Fig. 2, except the Keck 10 and 18 μm measurements, which are only for IRS-I-2.

[b] Astrometric reference for IR images; the 70 μm astrometry was bootstrapped from point sources in the shifted SOFIA 53 μm image.

[c] Data from Hunter et al. (2017)

[d] Augmented with extended configuration data from 2007-Aug-23 (2007A-S007) for a projected uv range = 30-577 kλ.

[e] Astrometric reference for SMA images

Figure 1

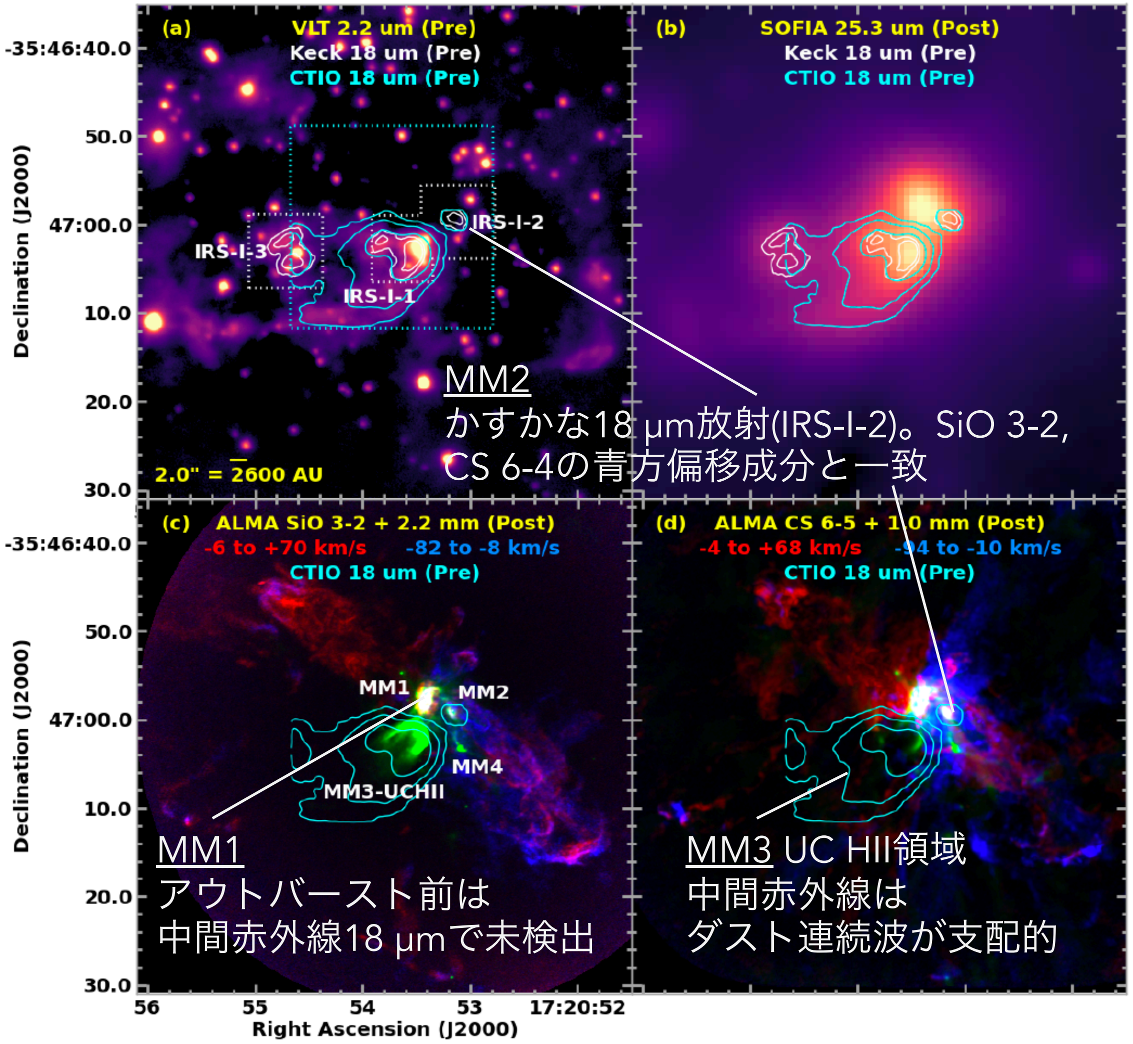

MM2
かすかな18 μm放射(IRS-I-2)。SiO 3-2, CS 6-4の青方偏移成分と一致

MM1
アウトバースト前は
中間赤外線18 μmで未検出

MM3 UC HII領域
中間赤外線は
ダスト連続波が支配的

Figure 2

ミリ波フラックスの比
MM1:MM2
2.1 (pre) → 10.5 (proto)

(c) spectral index $S_\nu \propto \nu^\alpha$ image
MM1, 2, 4はダスト連続波が支配的
MM1の一部とMM4はほぼoptically thick (**α**~2)
MM3は**α**~-0.1 optically thin free-free emission

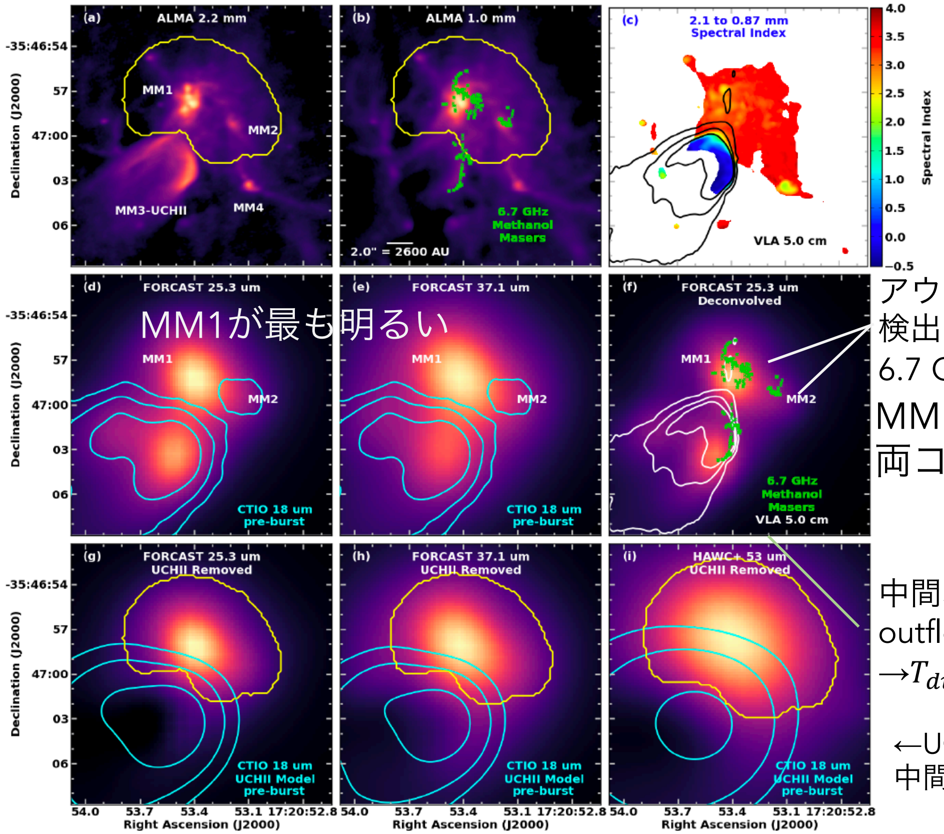

MM1が最も明るい

アウトバースト前には
検出されなかった
6.7 GHzメタノールメーザー
MM1とMM2
両コンポーネントがみえる

中間赤外線で明るい
outflow cavityをトレース
→$T_{dust} \geq 120\ K$を示唆

←UC HII領域の影響を除いた
中間赤外線画像

Figure 2. (a) ALMA 2.2 mm image with the four primary millimeter sources labeled; (b) ALMA 1.0 mm image; both (a) and (b) show the ALMA photometry aperture as a yellow contour. (c) spectral index image created from the images in (a) and (b), with black VLA 5 cm contours (0.15, 4.0, 13.2 mJy beam^{-1}) from Hunter et al. (2018). (d) and (e) FORCAST 25 and 37 μm images, overlaid with CTIO 18 μm contours (smoothed to 1.″2; 0.7, 1.75, 5.6 Jy beam^{-1}). (f) deconvolved 25 μm image ($\sim 2''$ resolution) with the 5 cm contours from (c). Fitted 6.7 GHz methanol maser positions from Hunter et al. (2018) are shown on panels (b) and (f). (g-i) 25, 37, and 53 μm images with the UCHII model removed, cyan contours of the 18 μm image smoothed to the SOFIA image resolutions, and photometry apertures in yellow (scaled in size as described in §3.2). All data were obtained post-outburst except the 18 μm contours in (d,e,g,h,i). Angular resolutions are provided in Table 2.

Figure 3

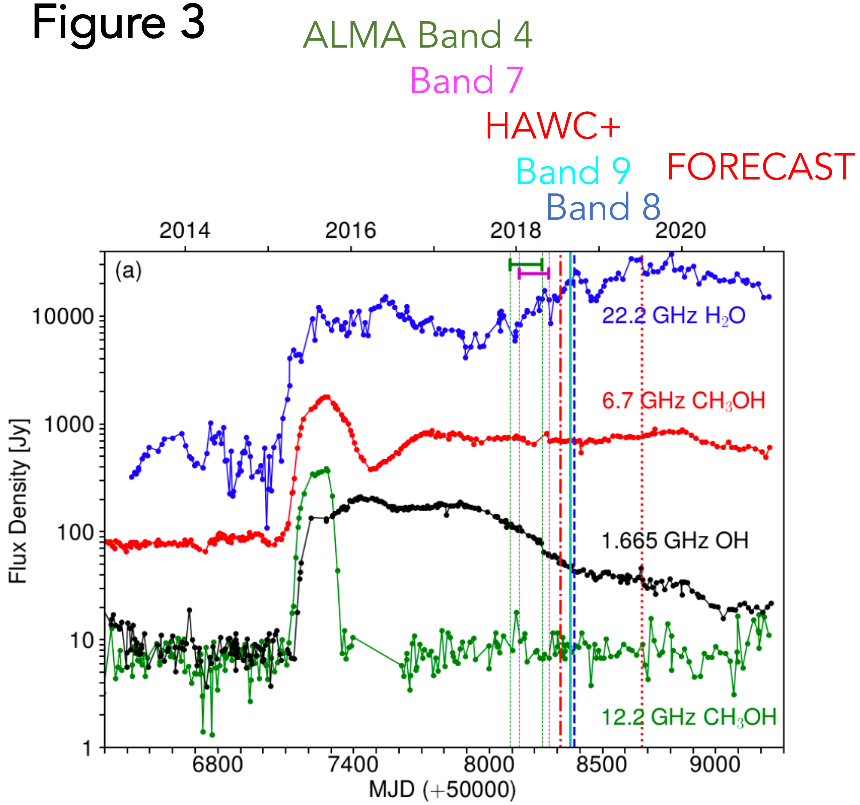

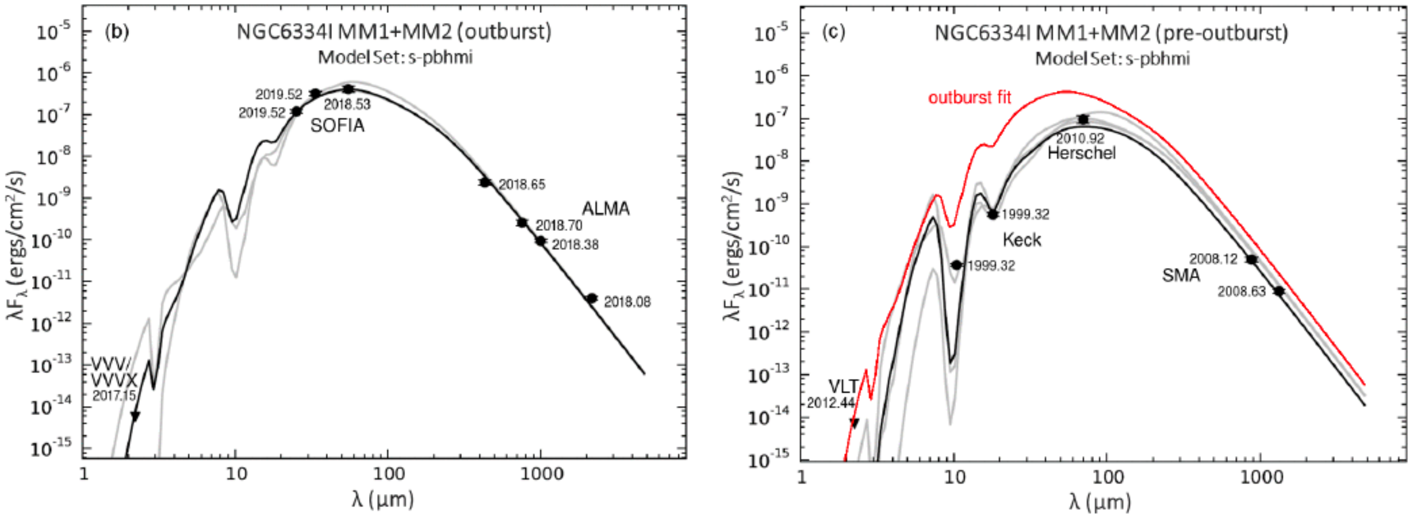

(a)メーザー放射のlight curve

- ✓ アウトバースト前にMM2とMM3で上昇
- ✓ 12.2 GHzのフレアは数ヶ月で消えた
- ✓ 6.7 GHzは未だ強い

(b:左) outburst SED+RT models (Robitaille 2017)
(c:右) **pre-**outburst SED+RT models 赤色は(b)のbest-fit

- ベストフィット(b)はoutflow cavityとpower-law envelopeをもつ $L_{\rm burst} = 49{,}000 \pm 8{,}000\ L_{\odot}$の中心星の場合に対応
- pre-outburstの場合(c)、アウトフロー の開口角が半分で $L_{\rm preburst} = 4{,}300 \pm 900\ L_{\odot}$に対応

MM1、MM2ともにホットコア分子($T_{\rm ex} = 150 - 200$ K)が検出されている大質量原始星をもつため、ミリ波のフラックス密度からLuminosity ratioを見積もった
→ $L_{\rm MM1,pre} = 2{,}900 \pm 600\ L_{\odot}$& $L_{\rm MM1,burst} = 47{,}600 \pm 7{,}800\ L_{\odot}$
比は16.3±4.4 (マグニチュード3のアウトバースト)

大質量原始星の全光度 (Meyer et al. 2021) $L = 4\pi R_{\mathrm{proto}}^2 \sigma T_{\mathrm{eff}}^4 + G M_* \dot{M}_{\mathrm{acc}} / R_{\mathrm{proto}}$ (1)
$L_{\mathrm{MM1,pre}}$の半分が太陽金属量をもつZAMS光球からくるとすると、
progenitorは$M_* = 6.7\ M_\odot, R_* = 2.6\ R_\odot, T_{\mathrm{eff}} = 22{,}000$ K (Tout et al. 1996)でB1.5VとB2Vの間
電離光子率は$Q = 2.1 \times 10^{44} \mathrm{phs}^{-1} > 1.7 \times 10^{44} \mathrm{phs}^{-1}$(HC HII領域MM1Bの1.3 cmフラックス密度を再現するのに必要な量)
→MM1BはMM1の光度の大部分に貢献している
光度の増加分$\Delta L = L_{MM1,burst} - L_{\mathrm{MM1,pre}} = 4{,}4700 \pm 7{,}900\ L_\odot$が全て降着起源だとすると、降着率は $6 \times 10^{-4} \left(R_{\mathrm{proto}} / 2.6\ R_\odot \right) M_\odot \mathrm{yr}^{-1}$

アウトバーストで獲得した質量~0.1-0.3 $M_\odot$、MM1Bアウトバーストの寿命~40-130年を示唆
継続時間($\Delta t > 6$ yr)を考慮すると全降着エネルギーは$E_{\mathrm{acc}} = \Delta L \Delta t > (3.2 \pm 0.6) \times 10^{39}$ J
他のバースト(S255IR-NIR3やG358.93-0.03)よりも継続時間もエネルギーも3倍
FU Ori (Class 0)のタイムスケールに似ている

本研究の結果は、様々な原始星質量のアウトバーストの研究の重要性、センチ波から中間赤外線までの進化を継続的にモニターすることの重要性を強調する

10. # Clustered star formation towards Berkeley 87 / ON2. I. Multi-wavelength census and the population overlap problem

Diego de la Fuente, Carlos G. Román-Zúñiga, Elena Jiménez-Bailón, João Alves, Miriam Garcia, Sean Venus

★ (ABRIDGED) Disentangling line-of-sight alignments of young stellar populations is crucial for observational studies of star-forming complexes. This task is particularly problematic in a Cygnus-X subregion where several components, located at different distances, are overlapped: the Berkeley 87 young massive cluster, the poorly-known [DB2001] Cl05 embedded cluster, and the ON2 star-forming complex, in turn composed of several HII regions. We aim at providing a methodology for building an exhaustive census of young objects that can consistently deal with large differences in both extinction and distance. OMEGA2000 near-infrared observations of the Berkeley 87 / ON2 field are merged with archival data from Gaia, Chandra, Spitzer, and Herschel, as well as cross-identifications from the literature. To address the incompleteness effects and selection biases that arise from the line-of-sight overlap, we adapt existing methods for extinction estimation and young object classification, and we define the intrinsic reddening index, R_{int}, a new tool to separate intrinsically red sources from those whose infrared color excess is caused by extinction. We also introduce a new method to find young stellar objects based on R_{int}. The flexibility of our approach allows to overcome photometric biases in order to obtain homogeneous catalogs of young sources. As a result, we find 571 objects whose classification is related to recent or ongoing star formation. Together with other point sources with individual estimates of distance or extinction, we compile a catalog of 3005 objects to be used for further membership work. A new distance for Berkeley 87, (1673 ± 17) pc, is estimated as a median of 13 spectroscopic members with accurate Gaia EDR3 parallaxes. Our multi-wavelength census will serve as a basis for disentangling the overlapped populations.

Cygnus-X subregionにおける、視線方向の複数成分の重なりによる問題を、近赤外線観測の減光から解決しようと試みた

本質的に赤い天体と、減光によって赤くなった天体を切り分ける指標R_{int}を定義し、若い星を見つける方法を確立

若い天体の均質なカタログを得ることができる。本手法により最近できた星や形成途中の星を571天体発見。距離や減光を個別に見積もった他の点源と合わせて3005天体のカタログを作成した。

12. Dispersal timescale of protoplanetary disks in the low-metallicity young cluster Dolidze 25

M. G. Guarcello, K. Biazzo, J. J. Drake, G. Micela, L. Prisinzano, S. Sciortino, F. Damiani, E. Flaccomio, C. Neiner, N. J. Wright ★ The dispersal of protoplanetary disks sets the timescale available for planets to assemble, and thus it is one of the fundamental parameters in theories of planetary formation. Disk dispersal is determined by several properties of the central star, the disk itself, and the surrounding environment. In particular, the metallicity of disks may impact their evolution, even if to date controversial results exist: in low-metallicity clusters disks seem to rapidly disperse, while in the Magellanic Clouds some evidence supports the existence of accreting disks few tens of Myrs old. In this paper we study the dispersal timescale of disks in Dolidze 25, the young cluster in proximity of the Sun with lowest metallicity, with the aim of understanding whether disk evolution is impacted by the low-metallicity of the cluster. We have analyzed Chandra/ACIS-I observations of the cluster and combined the resulting source catalog with existing optical and infrared catalogs of the region. We selected the disk-bearing population and the disk-less population of Dolidze 25. We have derived stellar parameters from isochrones fitted to color-magnitude diagrams. We derived a disk fraction of about 34existing estimates of the disk fraction of clusters younger than 10 Myrs, our study suggests that the disk fraction of Dolidze 25 is lower than what is expected from its age alone. Even if our results are not conclusive given the intrinsic uncertainty on stellar ages estimated from isochrones fitting to color-magnitude diagrams, we suggest that disk evolution in Dolidze 25 may be impacted by the environment. Given the poor O star population and low stellar density of the cluster, it is more likely that disks dispersal timescale is dictated more by the low metallicity of the cluster rather than external photoevaporation or dynamical encounters.

原始惑星系円盤の散逸は惑星が物質を集めるのに許される時間を決定するため、惑星形成論において基本的なパラメータ。
円盤散逸は中心星や円盤自身や周囲の環境などで決まるが、“円盤の金属量”も重要かもしれない。議論中

低金属量環境では、円盤は早く散逸する? 観測的はMagellanic Cloudsでは数十 Myrの降着円盤の証拠が示唆されている

Dolidze 25 (太陽に近接した若い星団で最も金属度が低い)の円盤の散逸タイムスケールを、Chandra/ACIS-I観測と可視/赤外のカタログから調べた→**円盤をもつ割合は~34 %、クラスターの年齢は1.2 Myr**。10 Myrより若いクラスターと比較すると、**年齢から予想されるより低い割合**だった。

Dolidze 25における円盤進化は環境に影響されている。O型星の少なさや星密度の低さを考慮すると、円盤の散逸タイムスケールは、光蒸発や動的な衝突ではなく低金属量によるのではないか。

13. **Analysis of physical processes in eruptive YSOs with near infrared spectra and multi-wavelength light curves**

Zhen Guo, P. W. Lucas, C. Contreras Peña, L. C. Smith, C. Morris, R. G. Kurtev, J. Borissova, J. Alonso-García, D. Minniti, A. -N. Chené, M. S. N. Kumar, A. Caratti o Garatti, D. Froebrich, W. H. Stimson ★

The decade-long Vista Variables in the Via Lactea (VVV) survey has detected numerous highly variable young stellar objects (YSOs). We present a study of 61 highly variable VVV YSOs (ΔK_s = 1-5 mag), combining near infrared spectra from Magellan and VLT with VVV and NEOWISE light curves to investigate physical mechanisms behind eruptive events. Most sources are spectroscopically confirmed as eruptive variables (typically Class I YSOs) but variable extinction is also seen. Among them, magnetically controlled accretion, identified by HI recombination emission (usually accompanied by CO emission), is observed in 46 YSOs. Boundary layer accretion, associated with FU Ori-like outbursts identified by CO overtone and H_2O absorption, is observed only in longer duration events (≥5 yr total duration). However, even in long duration events, the magnetically controlled accretion mode predominates, with amplitudes similar to the boundary layer mode. Shorter (100-700 days) eruptive events usually have lower amplitudes and these events are generally either periodic accretors or multiple timescale events, wherein large photometric changes occur on timescales of weeks and years. We find that the ratio of amplitudes in K_s and $W2$ can distinguish between variable accretion and variable extinction. Several YSOs are periodic or quasi-periodic variables. We identify examples of periodic accretors and extinction-driven periodicity among them (with periods up to 5 yr) though more data are needed to classify some cases. The data suggest that dynamic interactions with a companion may control the accretion rate in a substantial proportion of eruptive systems, although star-disc interactions should also be considered.

61個の変化の激しいVVV YSOs (ΔK_s=1-5 mag)について、噴出イベントの背景となる物理を調べた

46 YSOからはHI再結合線が同定され、磁場が支配的な降着が観測された。KsとW2の振幅の比が、variable accretionとvariable extinctionを切り分けるのに良い指標だと発見。

周期的な変動をするものもあった(最大5年)。伴星との力学的相互作用が降着率を制御していることを示唆。しかし、星ー円盤の相互作用も考える必要がある。

15. **Discovery of an Edge-on Circumstellar Debris Disk Around BD+45°598: a Newly Identifed Member of the β Pictoris Moving Group**

Sasha Hinkley, Elisabeth C. Matthews, Charlène Lefevre, Jean-Francois Lestrade, Grant Kennedy, Dimitri Mawet, Karl R. Stapelfeldt, Shrishmoy Ray, Eric Mamajek, Brendan P. Bowler, David Wilner, Jonathan Williams, Megan Ansdell, Mark Wyatt, Alexis Lau, Mark W. Phillips Jorge Fernandez Fernandez, Jonathan Gagné, Emma Bubb, Ben J. Sutlieff, Thomas J. G. Wilson, Brenda Matthews, Henry Ngo, Danielle Piskorz, Justin R. Crepp, Erica Gonzalez, Andrew W. Mann, Gregory Mace ★ We report the discovery of a circumstellar debris disk viewed nearly edge-on and associated with the young, K1 star BD+45°598 using high-contrast imaging at 2.2μm obtained at the W.M. Keck Observatory. We detect the disk in scattered light with a peak significance of $\sim 5\sigma$ over three epochs, and our best-fit model of the disk is an almost edge-on ~70 AU ring, with inclination angle ~87°. Using the NOEMA interferometer at the Plateau de Bure Observatory operating at 1.3mm, we find resolved continuum emission aligned with the ring structure seen in the 2.2μm images. We estimate a fractional infrared luminosity of $L_{IR}/L_{tot} \simeq 6^{+2}_{-1} \times 10^{-4}$, higher than that of the debris disk around AU Mic. Several characteristics of BD+45°598, such as its galactic space motion, placement in a color-magnitude diagram, and strong presence of Lithium, are all consistent with its membership in the β Pictoris Moving Group with an age of 23±3 Myr. However, the galactic position for BD+45°598 is slightly discrepant from previously-known members of the β Pictoris Moving Group, possibly indicating an extension of members of this moving group to distances of at least 70pc. BD+45°598 appears to be an example from a population of young circumstellar debris systems associated with newly identified members of young moving groups that can be imaged in scattered light, key objects for mapping out the early evolution of planetary systems from ~10-100 Myr. This target will also be ideal for northern-hemisphere, high-contrast imaging platforms to search for self-luminous, planetary mass companions residing in this system.

2.2 μmのhigh-contrast imagingにより、若い星K1 star BD+45°598に付随する**ほぼedge-onのデブリ円盤**を発見。~70 auのリング(傾き角~87°)。NOEMA 1.3mmでリングに沿った連続波放射を検出。L_{IR}/L_{tot}~6×10^{-4}でAU Mic周りのデブリ円盤より高い値を示した。様々な特徴は**β Pictoris Moving Group(~23 Myr)のメンバーと一致**するが、銀河系内での位置はわずかに異なっている。→70pc以上に広がっている可能性

~10-100 Myrの惑星系の初期進化を明らかにする上で重要な天体といえ、この系に存在する惑星質量のcompanionを探す北半球のhigh-contrast imaging platformとして理想的

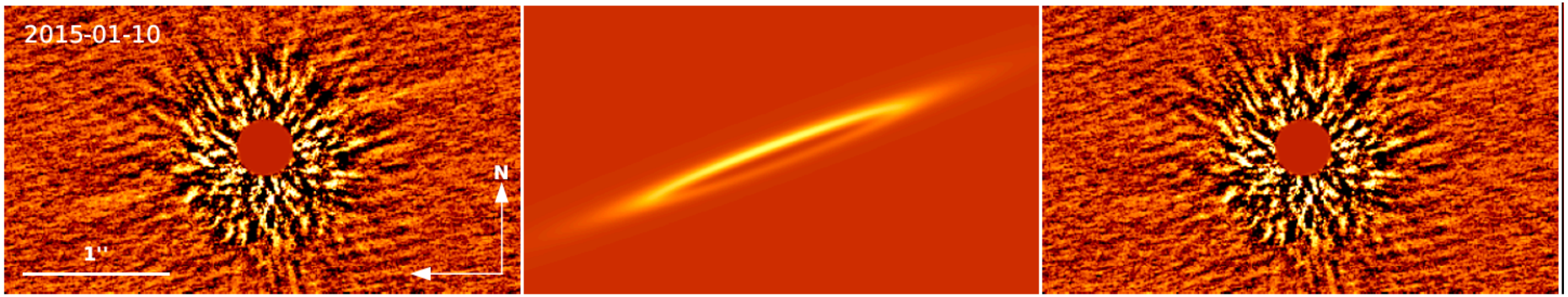

2.2 μm data best fit model Residual

NOEMA best fit model

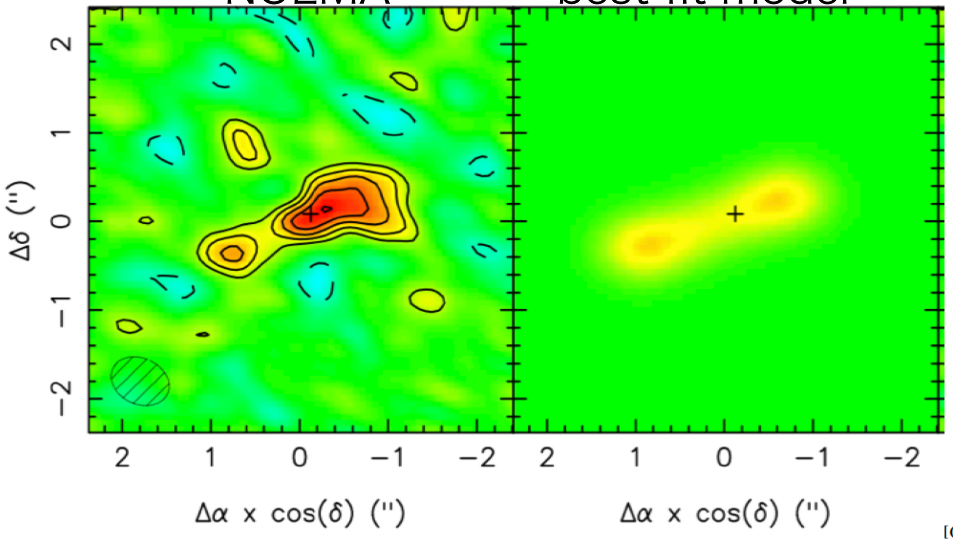

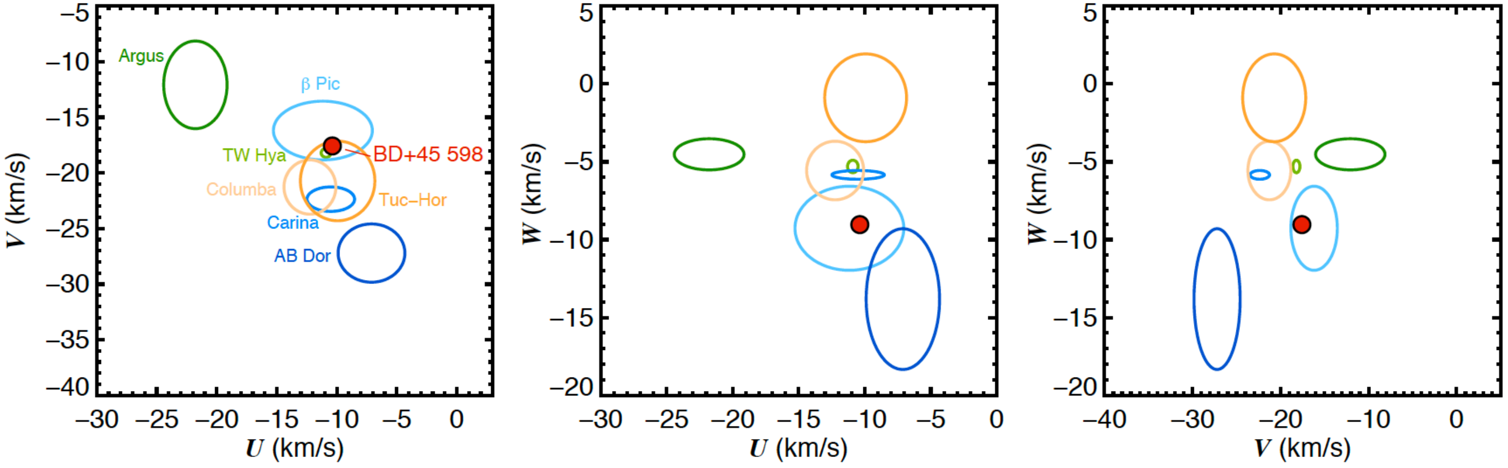

IG. 6.— The galactic space velocity representation for several nearby young moving groups (ellipses), as defined from Malo et al. (2014), except for TW Hya taken from Weinberger et al. (2013). The position of BD+45° 598 in this space is shown by the red point, and in all three projections is consistent with membership to the BPMG.

17. Long-term $V(RI)_c$ CCD photometry of pre-main-sequence stars in the association Cepheus OB3

Sunay Ibryamov, Gabriela Zidarova, Evgeni Semkov, Stoyanka Peneva ★ Results from optical CCD photometric observations of 13 pre-main-sequence stars collected during the period from February 2007 to November 2020 are presented. These stars are located in the association Cepheus OB3, in the field of the young star V733 Cephei. Photometric observations, especially concerning the long-term variability of the stars, are missing in the literature. We present the first long-term $V(RI)_c$ monitoring for them, that cover 13 years. Results from our study indicate that all of the investigated stars manifest strong photometric variability. The presented paper is a part of our program for the photometric study of PMS stars located in active star-forming regions.

Cepheus OB3にある13個の前主系列星のCCD 測光観測の結果(2007年2月から2020年11月)

すべての恒星が強い光度変動を示した

18. MRI-active inner regions of protoplanetary discs. I. A detailed model of disc structure

Marija R. Jankovic, James E. Owen, Subhanjoy Mohanty, Jonathan C. Tan ★ Short-period super-Earth-sized planets are common. Explaining how they form near their present orbits requires understanding the structure of the inner regions of protoplanetary discs. Previous studies have argued that the hot inner protoplanetary disc is unstable to the magneto-rotational instability (MRI) due to thermal ionization of potassium, and that a local gas pressure maximum forms at the outer edge of this MRI-active zone. Here we present a steady-state model for inner discs accreting viscously, primarily due to the MRI. The structure and MRI-viscosity of the inner disc are fully coupled in our model; moreover, we account for many processes omitted in previous such models, including disc heating by both accretion and stellar irradiation, vertical energy transport, realistic dust opacities, dust effects on disc ionization and non-thermal sources of ionization. For a disc around a solar-mass star with a standard gas accretion rate ($\dot{M}\sim10^{-8}\mathrm{M}_{\odot}\mathrm{yr}^{-1}$) and small dust grains, we find that the inner disc is optically thick, and the accretion heat is primarily released near the midplane. As a result, both the disc midplane temperature and the location of the pressure maximum are only marginally affected by stellar irradiation, and the inner disc is also convectively unstable. As previously suggested, the inner disc is primarily ionized through thermionic and potassium ion emission from dust grains, which, at high temperatures, counteract adsorption of free charges onto grains. Our results show that the location of the pressure maximum is determined by the threshold temperature above which thermionic and ion emission become efficient.

短周期super-Earth sizeの惑星がどのようにできたか。原始惑星系**円盤内側領域**の構造理解が必要

高温内側領域では、MRI不安定性に不安定で、MRI-active zoneの外側edgeで局所ガス圧が極大になる

内側円盤がMRIによって粘性降着する定常状態モデル(降着や中心性からの放射による円盤加熱、垂直方向の縁エルギー輸送、現実的なダストopacity、円盤電離や非熱的な電離源へのダストの影響など考慮)

→太陽質量程度の星周りの円盤($\dot{M}\sim10^{-8}\,M_{\odot}\mathrm{yr}^{-1}$、小さいダスト粒子)の内側円盤は光学的に厚く、降着加熱は中心面付近で解放される。中心面温度や圧力極大の位置は中心星の照射からわずかに影響を受け、内側円盤は対流不安定

圧力極大の位置は熱電子とイオン放射が効率的になる温度がしきい値となって決まる